Pergamon

PII: S0301-9322(96)00062-6

Int. J. Multiphase Flow Vol. 23, No. 1, pp. 113–129, 1997

0301-9322/97 $17.00 + 0.00

DISPLACEMENT OF ONE NEWTONIAN FLUID BY ANOTHER: DENSITY EFFECTS IN AXIAL ANNULAR FLOW

P. SZABO and O. HASSAGER

Department of Chemical Engineering, Technical University of Denmark (DTU), DK-2800 Lyngby, Denmark

(Received 26 August 1994; in revised form 18 August 1996)

Abstract—The arbitrary Lagrange–Euler (ALE) finite element technique is used to simulate 3-D displacement of two immiscible Newtonian fluids in vertical annular wells. For equally viscous fluids the effect of distinct fluid densities is investigated in the region of low to intermediate Reynolds numbers. Comparison with a simple theory for drainage of thin films is performed. It is found that recirculations deform the fluid–fluid interface significantly in situations dominated by buoyancy forces. Also, a deviation from the concentric annular geometry is shown to induce azimuthal transport of fluid. Finally, the efficiency of the displacement is analysed for various flow situation. Copyright © 1996 Elsevier Science Ltd.

Key Words: annular flow, finite elements, arbitrary Langrange–Euler kinematics, fluid–fluid displacement, buoyancy forces, displacement efficiency, film drainage

1. INTRODUCTION

The displacement of one fluid by another in annular geometries is an important process in connection with drilling of oil/gas-wells. The main reason for this is that the success of the primary cementing operation (see e.g. Moore 1974) is crucial in ensuring a long lasting production from the well. In the cementing process a displacing cement is pumped down the well and up in the annular region outside the casing where it displaces mud and other drilling fluids. The aim of this process is to provide zonal isolation in the wellbore, i.e. to prevent oil, gas or water in one zone to flow into another zone, the formation say.

Two key factors in selecting the cement properties are fluid rheology and density. In this work we will focus on the effects of a difference between the densities of the displacing fluid (cement) and the displaced fluid (mud, drilling fluids). In order to reduce the number of dimensionless parameters in the analysis the fluids will be assumed Newtonian with equal viscosity.

A denser displacing fluid is known to improve the result of the cementing operation (Lockyear *et al.* 1989; Jakobsen *et al.* 1991; Tehrani *et al.* 1993). For concentric annuli, this improvement appears to be due to a flattening of the interface. As a result of this flattening recirculations appear near the interface (Long 1991). For eccentric annuli a denser displacing fluid also induces azimuthal transport of fluid from the wide to the narrow part of the annular space. This also improves the cementing operation (Tehrani *et al.* 1992; 1993).

The experiments by Long (1991) and Tehrani *et al.* (1993) have initiated the present investigation. In their work they considered the displacement of one fluid by another in a vertical annular geometry with variable eccentricity and an inner radius of 80% of that of the outer casing. They used both Newtonian and non-Newtonian fluids.

Previous numerical simulations of fluid–fluid displacement (Graves and Collins 1981; Tehrani *et al.* 1992) have solved the two phase flow problem on a fixed mesh. In order to distinguish between the two phases, they define concentrations for the fluid constituents, and solve an advection equation for the concentrations. In this approach the phase boundary will not coincide with the mesh points. Thus the concentrations cannot be completely discontinuous, but the transitions take place across a very thin layer.

In this work we have decided to regard the displacement process as a system with two immiscible fluids. The present simulations therefore include a deformation of the computational domain as

well as a tracking of the fluid–fluid interface. The advantage here is the knowledge of the precise interface position at any time during the displacement. In addition we have considered the full three-dimensional displacement problem. A suitable numerical technique is the finite element method using an arbitrary Langrangian–Eulerian kinematic description (see, e.g. Hughes *et al.* 1981; Huerta and Liu 1988; Szabo 1994; Szabo and Hassager 1995).

2. THEORY

2.1. Geometry and non-dimensional groups

The formulation of a fluid mechanical problem equivalent to the experiments carried out by Long (1991) is outlined below.

A general eccentric annular geometry is sketched in figure 1. The geometrical quantities are: the inner radius, R_1, the outer radius, R_2 and the center difference, δ. Based on these variables, two non-dimensional quantities can be defined: the ratio, $\kappa = R_1/R_2$, between the radii and the eccentricity, $e = \delta/(R_2 - R_1)$. Also, we define a characteristic length, $h = R_2 - R_1$. For the two fluids we denote by ρ_1 and ρ_2 the densities of the displacing and the displaced fluid respectively. The viscosities μ_1 and μ_2 are similarly defined.

In the axial displacement problem there are two fluid phases in which the equations of continuity and motion must be fulfilled. Based on these equations four non-dimensional parameters are introduced in a natural way. The Reynolds number in fluid-phase m

$$\mathrm{Re}_m = \frac{h\bar{v}\rho_m}{\mu_m}, \quad m = 1, 2 \qquad [1]$$

where $\bar{v}$ is the average linear fluid velocity based on a constant volumetric flow-rate.

The buoyancy number as defined in Long (1991)

$$\mathrm{Bu} = \frac{(\rho_1 - \rho_2)gh^2}{\bar{v}\mu_1} \qquad [2]$$

as well as the viscosity ratio

$$\mathrm{N}_\mu = \frac{\mu_2}{\mu_1}. \qquad [3]$$

The Reynolds number is a measure of the inertial forces relative to the viscous forces. In the same way, the buoyancy number is a measure of the buoyancy forces relative to viscous forces.

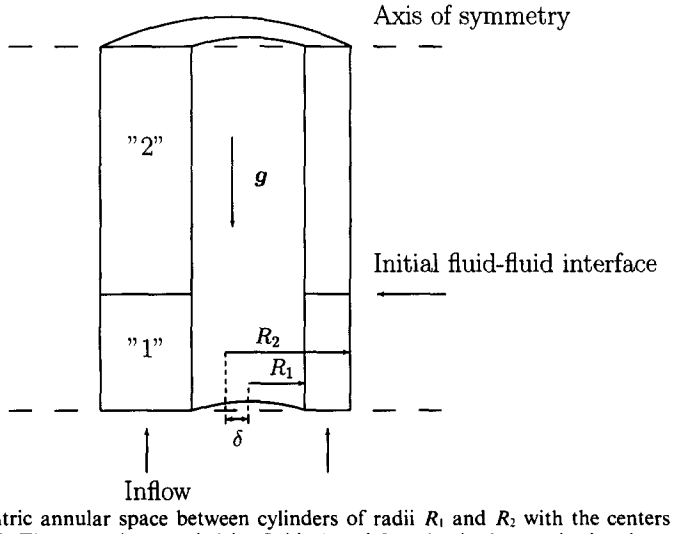

Figure 1. Eccentric annular space between cylinders of radii R_1 and R_2 with the centers displaced by a distance δ. The space is occupied by fluids 1 and 2 and $\boldsymbol{g}$ is the gravitational acceleration.

In addition the ratio of inertial forces to buoyancy forces is given by the Froude number defined here as

$$\mathrm{Fr} = \frac{\rho_1 \bar{v}^2}{(\rho_1 - \rho_2)gh} = \frac{\mathrm{Re}_1}{\mathrm{Bu}}. \qquad [4]$$

Note however that only two of the numbers Re_1, Bu, Fr may be chosen independently.

For simplicity, N_μ is chosen equal to unity in all numerical simulations. Moreover, the ratio between the two Reynolds numbers is held fixed in order to simplify the computational analysis further. Here $\mathrm{Re} = \mathrm{Re}_1 = 1.01\ \mathrm{Re}_2$.

It is for the displacement process convenient to define a macroscopic measure of the quality/efficiency, i.e. a way to quantify the amount of fluid from the displaced phase which is left behind the displacement front. One such nondimensional measure (Tehrani *et al.* 1993) for displacement in pipes can be written as,

$$E(t) = \frac{\int_A \min\{L, z(x, y, t)\}\, \mathrm{d}x\, \mathrm{d}y}{\int_0^L \int_A \mathrm{d}x\, \mathrm{d}y\, \mathrm{d}z}, \qquad [5]$$

where L is the length of an annular section, A is the cross-sectional area and $z(x, y, t)$ is the position of the interface measured from the entrance. In order to extract as much information as possible from [5] we introduce a dimensionless time $T^* = t\bar{v}/L$. Note that for plug flow T^* would be unity at the moment of breakthrough.

For future reference we consider the special situation of laminar flow of fluids of equal viscosity in a concentric annular geometry. Here we use the expression for the axial velocity (Bird *et al.* 1960) to obtain for the displacement efficiency

$$E(T^*) = \frac{2}{1 - \kappa^2} \int_\kappa^1 \min\left\{1, 2T^*\left(\frac{1 - u^2 + \eta \ln u}{1 + \kappa^2 - \eta}\right)\right\} u\, \mathrm{d}u \qquad [6]$$

where $\eta = -(1 - \kappa^2)/\ln(\kappa)$ is a constant. In particular we obtain the efficiency at breakthrough

$$E_B = \frac{1 + \kappa^2 - \eta}{2 - \eta(1 - \ln(\eta/2))}. \qquad [7]$$

This basic result for the concentric annulus is illustrated in figure 2 where we recognise the linearity until breakthrough (at $E_B \approx 0.67$ in simple laminar flow for $\kappa = 0.8$).

3. LUBRICATION THEORY FOR THIN DRAINING FILMS

The flow in the displacement process will typically consist of a fluid front region, possibly an intermediate region and a draining film region. The flow in the draining film region was analysed by Flumerfelt [4] with a lubrication theory. Based on this lubrication theory we wish to develop here an evolution equation for the thickness of the draining film $f(z, t)$.

We consider then the geometry in figure 3. The internal viscosity is μ_1 and the film viscosity is μ_2. The film thickness is denoted $f(z, t)$. It is assumed that two mechanisms are responsible for the draining of the film, a wall shear stress, and the density difference $\Delta\rho = \rho_1 - \rho_2$. The gravitational acceleration $\boldsymbol{g}$ acts in the negative z-direction. Quasisteady motion in the film is assumed. In addition we assume that the shear stress on the phase boundary is the result merely of the flow in the interior phase, and can be calculated from that flow alone. Thus the local relation between shear stress and volume flow rate is that for laminar slit flow with viscosity μ_1.

The transient development of the film thickness is then given by the following quasilinear first order partial differential equation:

$$\frac{\partial f}{\partial t} + (\alpha f + \beta f^2)\frac{\partial f}{\partial z} = 0, \qquad [8]$$

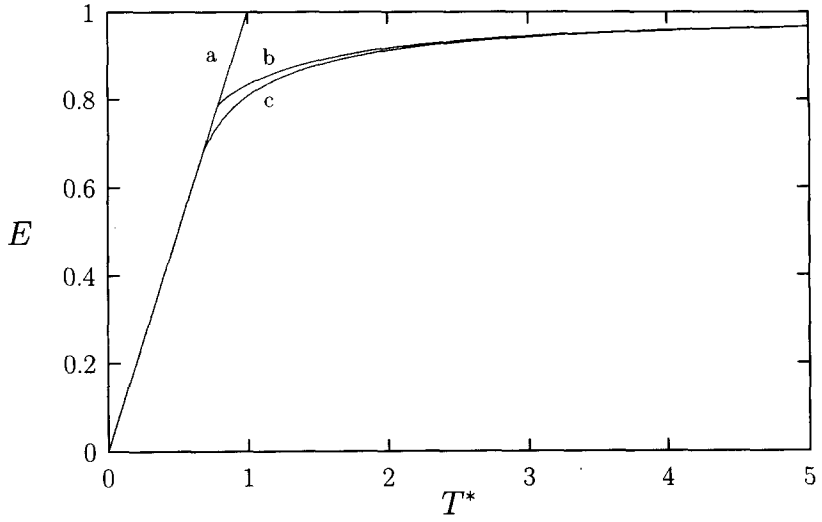

Figure 2. The displacement efficiency, E vs a dimensionless time T^*. Linear approach from naught to one indicate plug flow (curve a) whereas passive displacement (curve b) in laminar flow achieves an efficiency close to one only for very large times. For comparison the curve produced by the lubrication theory in section 3 is given as curve c.

where

$$\alpha = \frac{6\bar{v}\mu_1}{h\mu_2}, \quad \beta = \frac{\Delta\rho g}{\mu_2}. \qquad [9]$$

A general solution for $f(z, t)$ may be obtained for a boundary condition in the form:

$$f(z, 0) = f_0(z), \quad f_0(0) = 0.$$

This condition implies that the film thickness is zero at the entrance, so there is no inflow of phase 2.

A key element in the determination of the properties of the solution to the lubrication model [8] lies in the establishment of the characteristics [3]. We denote the parameter along the characteristics s. The equations to be integrated along the characteristics are then:

$$\frac{dt}{ds} = 1 \qquad [10]$$

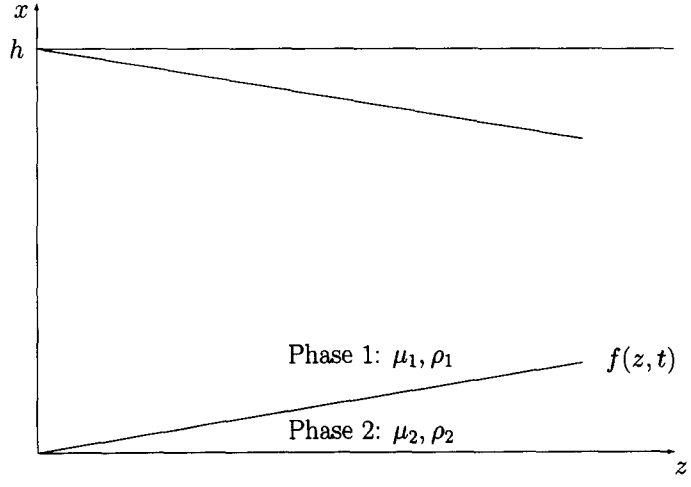

Figure 3. Defining sketch for the lubrication theory in section 3.

$$\frac{dz}{ds} = \alpha f + \beta f^2 \qquad [11]$$

$$\frac{df}{ds} = 0. \qquad [12]$$

The characteristics are given by

$$z = (\alpha f_0(z_0) + \beta f_0^2(z_0))t + z_0.$$

Note that f does not change along a characteristic. Furthermore, note that the characteristics are straight lines in the (z, t) plane. This means, that a given film thickness propagates with constant velocity.

As long as $f_0(z_0)$ is an increasing function the characteristics do not intersect, and the solution may be expressed implicitly as

$$f(z, t) = f_0(z - (\alpha f + \beta f^2)t.$$

We now wish to find an expression for the relative amount of initial fluid left in a given annulus of length L. One key reason why that can be defined is that the initial conditions become less important with increasing time. To illustrate this point, assume the specific initial profile $f_0(z) = \gamma z$. We then obtain for the solution

$$z = f(z, t)/\gamma + (\alpha f(z, t) + \beta f^2(z, t))t).$$

It follows that for large values of t and fixed γ we may to a good approximation use:

$$z = (\alpha f(z, t) + \beta f^2(z, t)t. \qquad [13]$$

In particular we obtain for a fixed "large" value $z = L$:

$$L = (\alpha f(L, t) + \beta f^2(L, t))t. \qquad [14]$$

The relative volume of the displacer in the annulus, $E(t)$ defined in [5] may be obtained from a volume consideration: a volume consideration shows that

$$2BLW(1 - E(t)) = 2\left(Lf(z, t) - \int_0^{f(L,t)} z \, df(z, t)\right)W.$$

Here W is the length in the transverse direction. By introducing [13] we obtain:

$$1 - E(t) = \frac{f(L, t)}{B} - \frac{1}{BL}\left(\frac{1}{2}\alpha h^2(L, t) + \frac{1}{3}\beta f^3(L, t)\right)t.$$

We may now use [14] to eliminate t/L as follows:

$$1 - E(t) = \frac{f(L, t)}{B} - \frac{1}{B}\frac{\left(\frac{1}{2}\alpha f^2(L, t) + \frac{1}{3}\beta f^3(L, t)\right)}{\alpha f(L, t) + \beta f^2(L, t)}.$$

After some algebraic manipulations this may be simplified to:

$$1 - E(t) = \frac{\left(1 + \frac{2}{9}\mathrm{BuN}_\mu y\right)y}{1 + \frac{1}{6}\mathrm{BuN}_\mu} \qquad [15]$$

where $y = f(L, t)/h$ is the nondimensional film thickness at $z = L$.

Finally we need to solve for $f(L, t)$ in [14]. The solution may be expressed as follows:

$$y = \frac{3}{\mathrm{BuN}_\mu}\left(\sqrt{1 + \frac{\mathrm{BuN}_\mu^2}{9T^*}} - 1\right). \qquad [16]$$

Here the nondimensional time, T^* is defined as in section 2.1.

Thus in summary, the displacement efficiency is simply given by [15] and [16]. In particular we see that:

- The displacement efficiency does not depend on the ratio L/h, as long as $L/h \gg 1$.
- The displacement efficiency does not in this theory depend on the Reynolds number.
- For large T^* the viscosity ratio becomes more important than the buoyancy number in the determination of the efficiency.

The lubrication model above can be expected to provide a reasonable description for the flow behind the front. Thus, the result for $E(t)$ should be applied really only for $T^* > 1$.

4. THE FINITE ELEMENT MODEL

4.1. *Governing equations in the ALE description*

The equation of motion referred to an observation point moving with velocity $\mathbf{w}$ is (for reference see Lamb 1995 ([12.5]) or Szabo and Hassager 1995)

$$\rho_m\left(\frac{\partial \mathbf{v}}{\partial t} + (\mathbf{v} - \mathbf{w})\cdot(\nabla \mathbf{v})_{x=z}\right) = -\nabla p + \mu_m \nabla^2 \mathbf{v} + \rho_m \mathbf{g}. \quad [17]$$

In the same notation we write for the equation of continuity for an incompressible fluid

$$(\nabla \cdot \mathbf{v})_{x=z} = 0. \quad [18]$$

Equations [17] and [18] are used augmented by the definition of $\mathbf{w}$:

$$\mathbf{w}(\xi, t) = \frac{\partial}{\partial t}(\mathbf{z}(\xi, t)) \quad [19]$$

where $\mathbf{z}(\xi, t)$ is a particular path labeled by ξ.

The formulation includes the following situations: $\mathbf{w} = \mathbf{0}$ and $\mathbf{w} = \mathbf{v}$ gives the Euler and Lagrange formulations respectively whereas $\mathbf{w} = \mathbf{w}_0 \neq \{\mathbf{0}, \mathbf{v}\}$ is the ALE formulation. The space discretization of [17] and [18] follows the mixed Galerkin finite element method (for reference see Brezzi and Fortin 1991 or Zienkiewicz and Morgan 1983) with trilinear velocity shape functions and constant pressure approximations in each element. In addition the time discretization follows a fully implicit first order finite difference scheme.

The resulting system of non-linear algebraic equations is solved with a full Newton–Raphson technique that accounts for the moving grid positions due to the ALE formulation (Szabo and Hassager 1995).

4.2. *Automatic mesh displacement in time*

Two alternative methods have been used to control the deformation of the computational grid: an active semi-Lagrangian technique (Huerta and Liu 1988; Szabo and Hassager 1995) that ties into the implicit time-integration and a passive strategy that uses the velocity of a previous time-step to determine the new node positions.

The active semi-Lagrangian technique is formulated as a general linear transformation of the current velocity field, whence

$$w_k^i(t) = \sum_{m=1}^{3} \alpha_{mk}^i v_m^i(t), \quad \alpha_{mk}^i \in [0;1] \quad [20]$$

where i and $\{m, k\}$ denote the node index and the vectorial directions, respectively.

A pure Lagrange formulation is obtained when the $\alpha_{mk}^i = \delta_{mk}$ for all i. Also, it is possible to let the $\alpha_{mk}^i = \delta_{mk}$ for the nodes at the interface only, and then let the non zero components of α_{mk}^i decrease smoothly away from the interface.

The passive strategy is a simple way of smoothing out the mesh deformations, for instance behind moving interfaces. The concept is to point out a node j which may be located at the fluid–fluid

interface. Subsequently another node i can be made to move relative to this interface node j. The mesh velocity of node i is obtained as the velocity of node j multiplied by some weight factor. In order to simplify the computations the velocity of node j at the previous time-step, $t - \Delta t$, is used. Formally, the scheme reads

$$w^i_{o,k}(t) = \beta^i_k v^{j(i)}_k (t - \Delta t) \quad [21]$$

where β^i_k are constant during a time-step. The function $j(i)$ simply specifies the node j that node i depends on.

4.3. *Displacement in non-dimensional form*

A way of reducing the complexity of the problem is to introduce a modified pressure, $\mathscr{P}$, based on the hydrostatic pressure in fluid-phase 2, i.e. the displaced fluid. More precisely, this variable substitution implies that

$$-\nabla\mathscr{P} = -\nabla p + \rho_2 \mathbf{g}. \quad [22]$$

It is convenient to introduce the following non-dimensional variables in the model: $\mathbf{v}^* = \mathbf{v}/\bar{v}$, $\mathbf{w}^* = \mathbf{w}/\bar{v}$, $t^* = t\bar{v}/h$, $\boldsymbol{\chi} = \mathbf{g}/g$ and $\mathscr{P}^* = \mathscr{P}h/(\mu_2\bar{v})$. Here h is the gap-width in a concentric annular geometry and $\bar{v} = Q/(\pi R_2^2(1-\kappa^2))$ is the average linear velocity, i.e. the volumetric flow-rate divided by the cross-sectional area of the annulus. The result of this non-dimensionalisation of the equations of motion is:

in fluid-phase 1

$$\mathrm{Re}_1\left(\frac{\partial \mathbf{v}^*}{\partial t^*} + (\mathbf{v}^* - \mathbf{w}^*)\cdot(\nabla^*\mathbf{v}^*)_{x=z}\right) = -\mathrm{N}_\mu \nabla^*\mathscr{P}^* + \nabla^{*2}\mathbf{v}^* + \mathrm{Bu}\boldsymbol{\chi} \quad [23]$$

and in fluid-phase 2

$$\mathrm{Re}_2\left(\frac{\partial \mathbf{v}^*}{\partial t^*} + (\mathbf{v}^* - \mathbf{w}^*)\cdot(\nabla^*\mathbf{v}^*)_{x=z}\right) = -\nabla^*\mathscr{P}^* + \nabla^{*2}\mathbf{v}^*. \quad [24]$$

Here Bu, Re_1, Re_2 and N_μ are defined as in section 2.1.

Furthermore, the non-dimensional equation of continuity must be fulfilled in each fluid phase, whence

$$(\nabla^*\cdot\mathbf{v}^*)_{x=z} = 0. \quad [25]$$

5. SIMULATION RESULTS AND DISCUSSION

In order to establish a well specified mathematical problem, we introduce a set of boundary conditions. These are: no slip (i.e. $\mathbf{v} = \mathbf{0}$) at solid walls and no flow perpendicular to the annular symmetry plane (defined in figure 1) which however excludes possible helical solutions and the symmetry breaking gravity driven interfacial instability that Tehrani *et al.* (1992, 1993) have observed. The inflow is specified as the fully developed single fluid velocity field (of fluid 1) based on a constant volumetric flow rate (this velocity field is both in concentric and eccentric annular geometries computed with a 2-D finite element solver) and a vanishing pressure is imposed at a plane surface far downstream the interface. The boundary conditions mean that the displacing fluid is "pinned" at its initial position at $z = 0$ for all times. Thus we do not use a model for a moving contact point. This is in agreement with the lubrication theory in section 3. At the interface between the two fluids continuity of velocity and momentum flux is used. Thus there is no interfacial tension included.

Three different finite element meshes were used for the simulations. These are (axial elements × radial elements × azimuthal elements): 115 × 8 × 6 (MESH 1), 115 × 16 × 6 (MESH 2) and 115 × 16 × 12 (MESH 3). MESH 1 and MESH 2 were used for the concentric simulations whereas MESH 3 was used in the eccentric simulations. Although no rigorous convergence results have been produced on these meshes the meshes were refined until a smooth solution was obtained. More precisely the large axial number of elements were necessary at intermediate Reynolds numbers both to resolve the interface region and to eliminate numerical

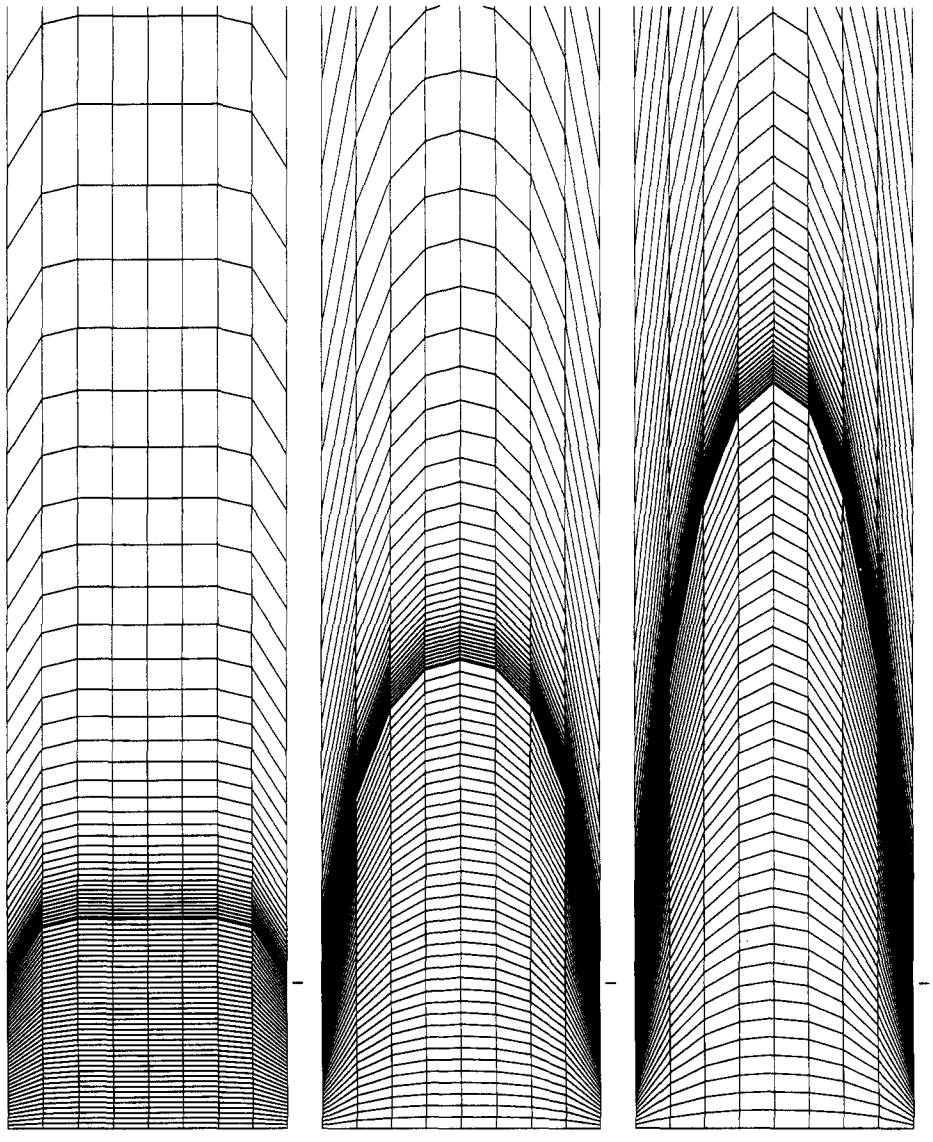

Figure 4. The zx-part of the interfacial area in MESH 1. The figure shows the mesh as it deforms during time. As a measure of the deformation is used the axial movement, Δz_f, of the centernode at the interface. (a) $t^* = 1.06$, $\Delta z_f = 1.3h$, (b) $t^* = 4.6$, $\Delta z_f = 6.6h$, and (c) $t^* = 8.13$. The horizontal line right to the meshes indicates the position of the interface node on the wall.

oscillations. Furthermore, large buoyancy numbers required a finer resolution across the annular gap (MESH 2 and MESH 3).

In order to illustrate the mesh discretisation and the deformations therein we have drawn the interface region in a deforming mesh during time integration. In figure 4 for MESH 1 with Re = 128 and Bu = 0.4 (Fr = 320).

The smooth deformation of the mesh in figure 4 is obtained with the semi-Lagrange technique defined in [20]. This is possible because there are no recirculations at Bu = 0.4 (Fr = 320). At larger values of Bu (especially at Bu = 400 or Fr = 0.32) the technique in [21] is used to decouple the flow field from the node displacements, except at the interface where nodes are Lagrangian.

5.1. *Flow in a concentric annulus*

5.1.1. Dynamic shape of the interface. According to experiments by Long (1991) an increasing buoyancy number induces strong recirculations in the vicinity of the moving interface for Reynolds numbers about 130. On the contrary the uni-directional flow seems to be stabilised at low and high Reynolds numbers (Re < 50 and Re > 400). For convenience a Reynolds number of 128 was chosen as the starting point for our simulations.

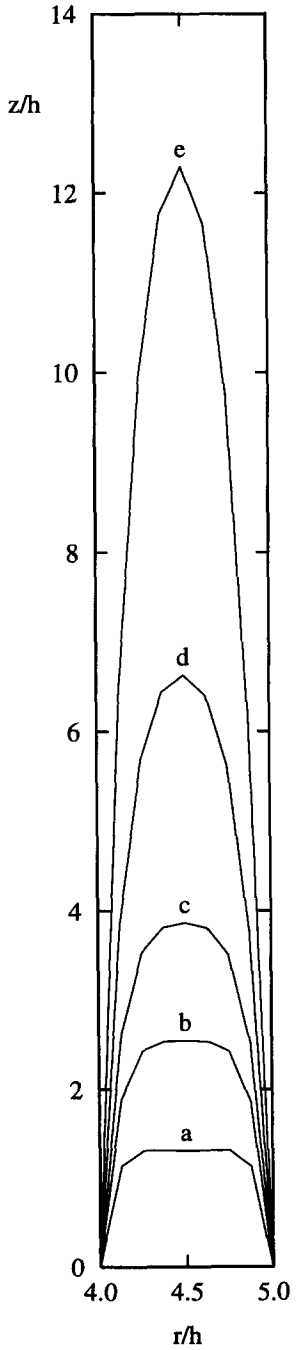

Figure 5. Concentric interface at Re = 128, Bu = 0.4 and Fr = 320 (MESH 1). (a) $t^* = 1.06$, (b) $t^* = 1.95$, (c) $t^* = 2.83$, (d) $t^* = 4.60$ and (e) $t^* = 8.13$.

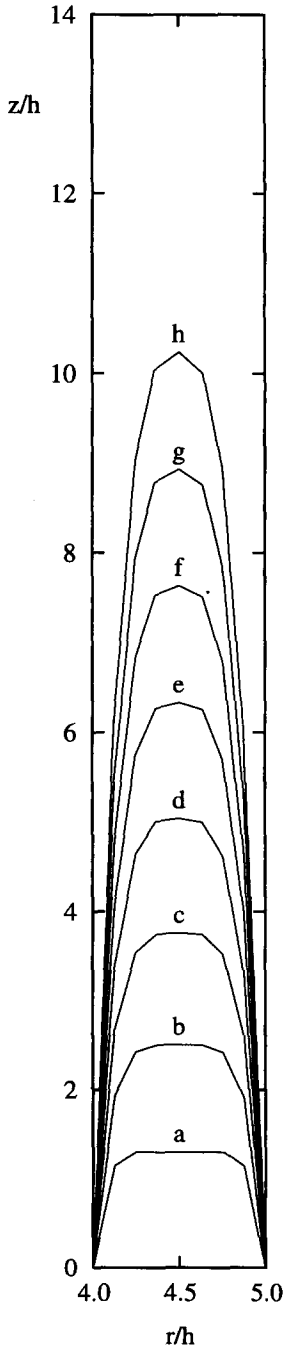

Figure 6. Concentric interface at Re = 128, Bu = 40 and Fr = 3.2 (MESH 1). (a) $t^* = 1.06$, (b) $t^* = 1.95$, (c) $t^* = 2.83$, (d) $t^* = 3.71$, (e) $t^* = 4.60$, (f) $t^* = 5.48$, (g) $t^* = 6.37$ and (h) $t^* = 7.25$.

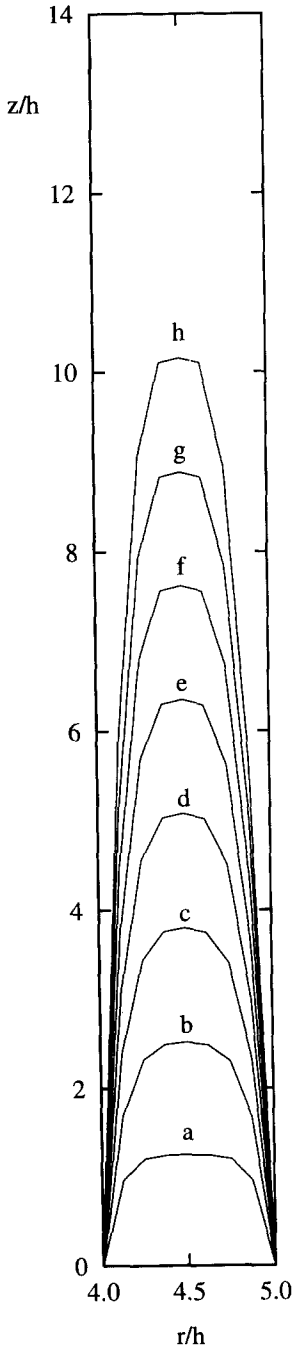

Figure 7. Concentric interface at Re = 64, Bu = 40 and Fr = 1.6 (MESH 1). (a) $t^* = 1.06$, (b) $t^* = 1.95$, (c) $t^* = 2.83$, (d) $t^* = 3.71$, (e) $t^* = 4.60$, (f) $t^* = 5.48$, (g) $t^* = 6.37$ and (h) $t^* = 7.25$.

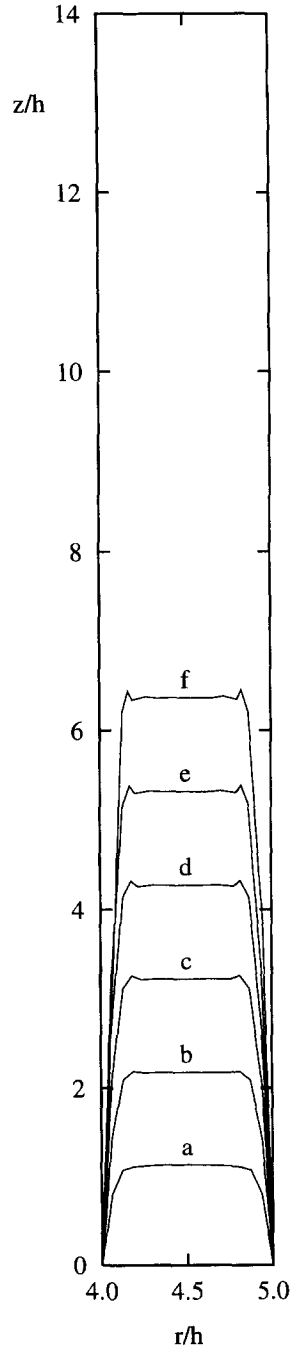

Figure 8. Concentric interface at Re = 128, Bu = 400 and Fr = 0.32 (MESH 2). (a) $t^* = 1.06$, (b) $t^* = 1.86$, (c) $t^* = 2.74$, (d) $t^* = 3.63$, (e) $t^* = 4.51$ and (f) $t^* = 5.39$.

At very low values of Bu a characteristic Poiseuille like interface evolves in time. An illustration is given in figure 5. This is not surprising since Bu = 0 corresponds to two identical fluids. If the buoyancy number is increased to about 40 (Fr = 3.2) the interface seems to be more flat at the front as shown in figure 6 but no steady interface shape seems to appear. By lowering the Reynolds number to 64 (Fr = 1.6) the interface seems to become more flat as indicated in figure 7. The fact that the shape of the interface front eventually becomes steady at large buoyancy numbers is apparent from figure 8 showing the interface at Re = 128 and Bu = 400 (Fr = 0.32).

5.1.2. Secondary flow near the moving interface. The velocity field close to the interface when Re = 128 and Bu = 400 (Fr = 0.32) is illustrated in figure 9. The vector field drawn is the current fluid velocity minus the velocity of the centerpoint at the interface. This procedure illustrates the eventually steady interface shape. Moreover one observes strong recirculations that in front of the interface transports fluid from the wall region to the center of the domain whereas fluid behind the interface is moved from the center to the wall region. In addition small recirculations appear near the interface front. The strong recirculations can be understood from mass conservation and

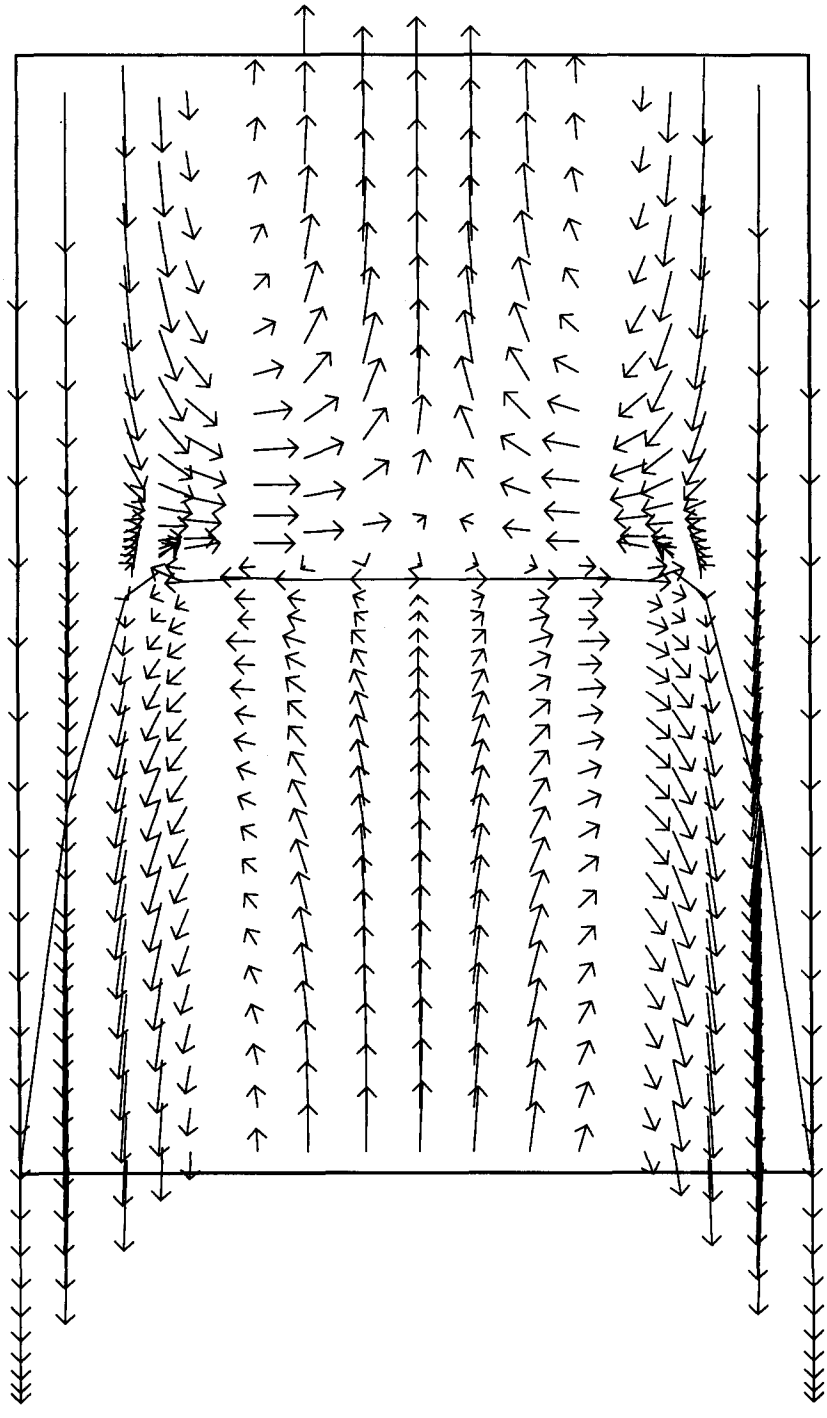

Figure 9. The secondary flow near the interface at Re = 128, Bu = 400, Fr = 0.32 and $t^* = 4.51$ (compare with figure 8(e)).

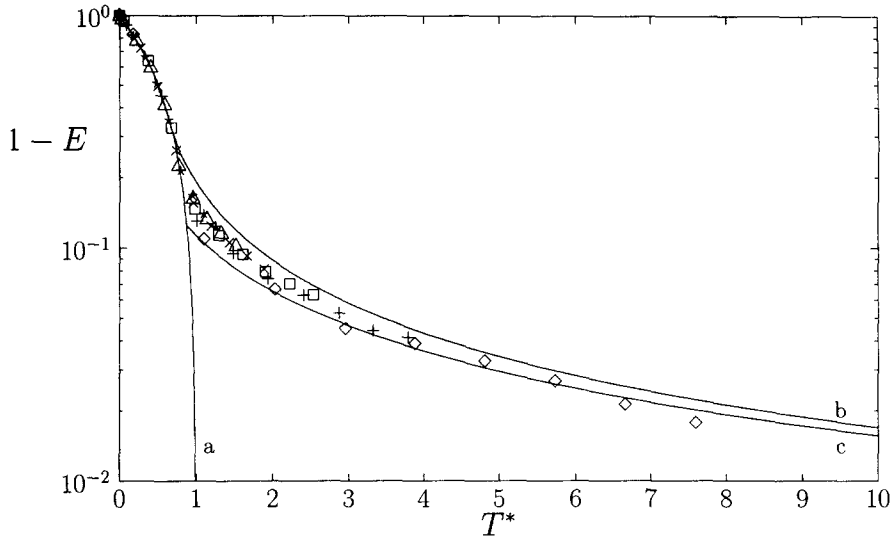

Figure 10. The displacement function, $1 - E$ vs a dimensionless time T^*: Re = 128, Bu = 40, Fr = 3.2 and $e = 0$. The symbols denote results from calculations with different values of L (see [5] for reference). $\diamond$: $L = h$, $+$: $L = 2h$, $\square$: $L = 3h$, $\times$: $L = 4h$, $\triangle$: $L = 5h$ and $*$: $L = 6h$. The curves denoted by (a) and (b) represent displacement in plug flow and in Poiseuille flow, respectively, whereas curve (c) is produced by the theory in section 3.

boundary conditions as follows. Downstream of the interface, the velocity profile is parabolic while the interface is flat. This necessarily induces flow from the centerplane towards the walls below the interface. A similar argument shows that there is flow from the walls towards the centerplane above the interface. The flow from the centerplane towards the walls below the interface and the opposing flow above the interface are connected by a fairly flat recirculation zone. The kinks near the corners are probably due to insufficient resolution of this secondary flow.

5.1.3. Displacement efficiency. As described in section 2.1 the nondimensional measure, $E(T^*)$ is a suitable quantity to determine. In order to extract as much information as possible we plot the logarithm of $1 - E$ vs T^*. This allows for a more precise comparison between different curves. In figure 10 we show the results of numerical computations at Re = 128 and Bu = 40 (Fr = 3.2) in a concentric annulus (with $\kappa = 0.8$). In the plot we have a curve that tends to zero when T^* approaches unity. This is the curve for plug flow. The upper curve represents simple laminar flow

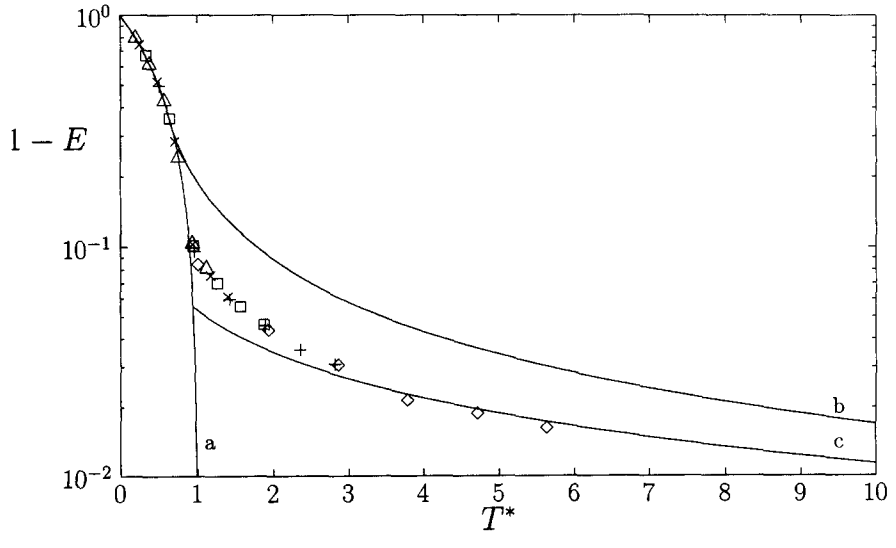

Figure 11. The displacement function, $1 - E$ vs a dimensionless time T^*: Re = 128, Bu = 400, Fr = 0.32 and $e = 0$. Symbols are defined as in figure 10.

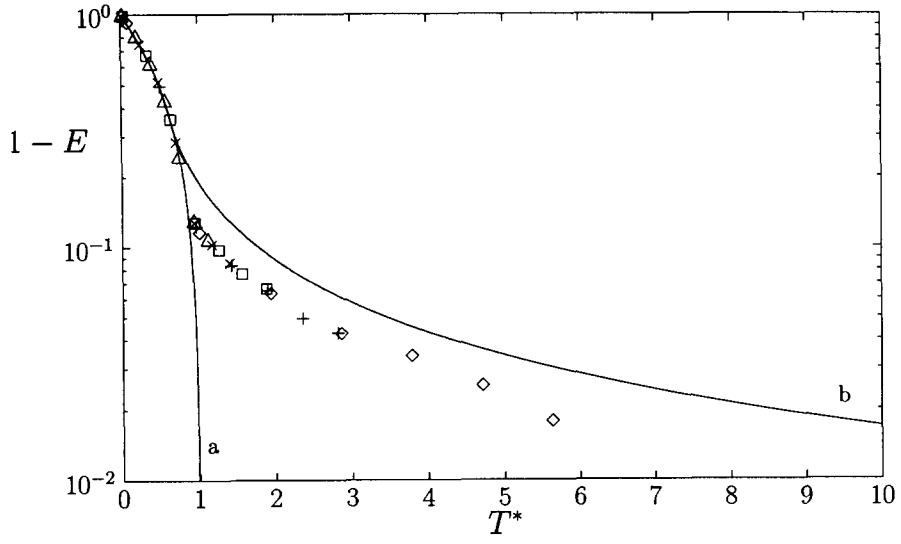

Figure 12. The displacement function, $1 - E$ vs a dimensionless time T^*: Re = 64, Bu = 400, Fr = 0.16 and $e = 0$. Symbols are defined as in figure 10.

(Poiseuille flow) whereas the lower curve is calculated using the lubrication theory in section 3. Note that the curves for Poiseuille flow and the lubrication prediction for Bu = 40 are relatively close. This indicates to us, that even at a buoyancy number of 40 the flow is largely unmodified by the density contrast. Furthermore, the numerical results fall between the two analytical results.

With respect to accuracy of the numerical results, we believe the main difficulty is in the resolution of the lubrication boundary layers near the walls. We take the fairly good agreement between the two idealized analytical results and the numerical results in figure 10 as a support for the mesh resolution.

According to the lubrication theory in section 3 the numerical results should have a collective curve provided $L/h \gg 1$. We believe that the scatter in figure 10 is due to the condition $L/h \gg 1$ being violated for some points.

By increasing the Buoyancy number (e.g. enlarging the density difference) to 400 (Fr = 0.32) we observe a qualitative change in the evolution of the efficiency. The plot in figure 11 shows that the displacement becomes more effective (the breakthrough occurs at a higher effectivity) and also, there now seems to be a clear collective curve for various values of L in agreement with the lubrication theory. This indicates a quasi steady-state displacement, i.e. that the interface front has attained a steady shape with a thin developing shear layer near the wall (like a thin layer lubricating the transport of a plug). For comparison we note that it is necessary to use only half (almost exactly!) as much of the displacing fluid when Re = 128 and Bu = 400 as for Bu = 0. If we lower the Reynolds number to 64 (so that Fr = 0.18) as in figure 12 we observe a significant change in the displacement efficiency. At Bu = 400 a lower Reynolds number seems to produce a thicker film layer near the wall and thence a lower efficiency than a larger value of Re.

The existence of a collective curve for the displacement efficiency would indicate that the shape of the interface scales with the total volume of fluid pumped. This has some far-reaching consequences. In practical cementing operations a ratio of $L/h \sim 0(10^4)$ is not unrealistic, while experiments and numerical simulations will be limited to much lower values. The scaling of the interface means that experiments and simulations for $L/h \sim 0(10^2)$ would be sufficient to predict behaviour in practical cementing operations.

5.2. Flow in an eccentric annulus

5.2.1. Azimuthal transport of fluid at large buoyancy numbers. In a situation where the difference in fluid densities is negligible (Bu $\approx$ 0) then uni-directional flow is maintained for some time even at non-zero Reynolds numbers as illustrated in figure 13.

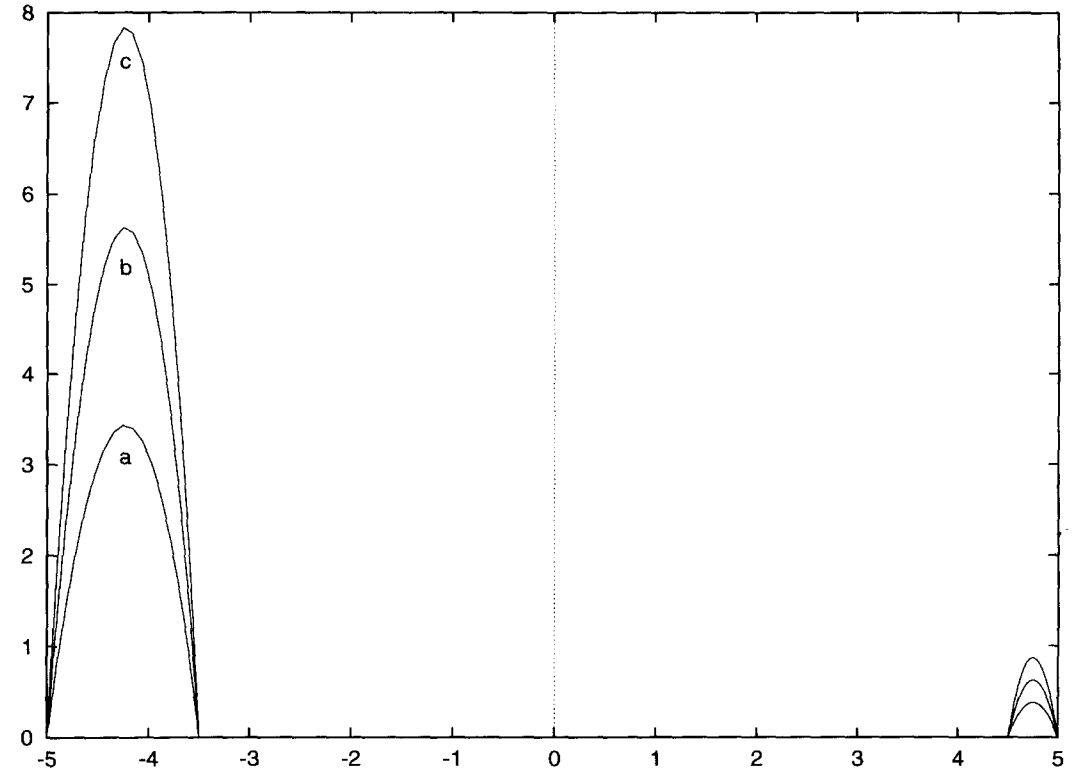

Figure 13. The development of the interface front for Re = 0, Bu = 0 and $e = 0.20$ (MESH 3): (a) $t^* = 1.38$, (b) $t^* = 2.26$ and (c) $t^* = 3.15$.

If the density difference is large the simulations show that a significant amount of fluid is transported in the azimuthal direction. This supports the observations by Tehrani *et al.* (1993). This is illustrated in figure 14 where the development of the interface front is illustrated for Bu = 400, Re = 128 and $e = 0.20$.

Therefore one important effect of a large buoyancy number is a relative reduction of the axial velocity in the wide part of the annulus in combination with a relative increase of the axial velocity in the narrow part of the geometry. The central part of the flow domain dominated by buoyancy

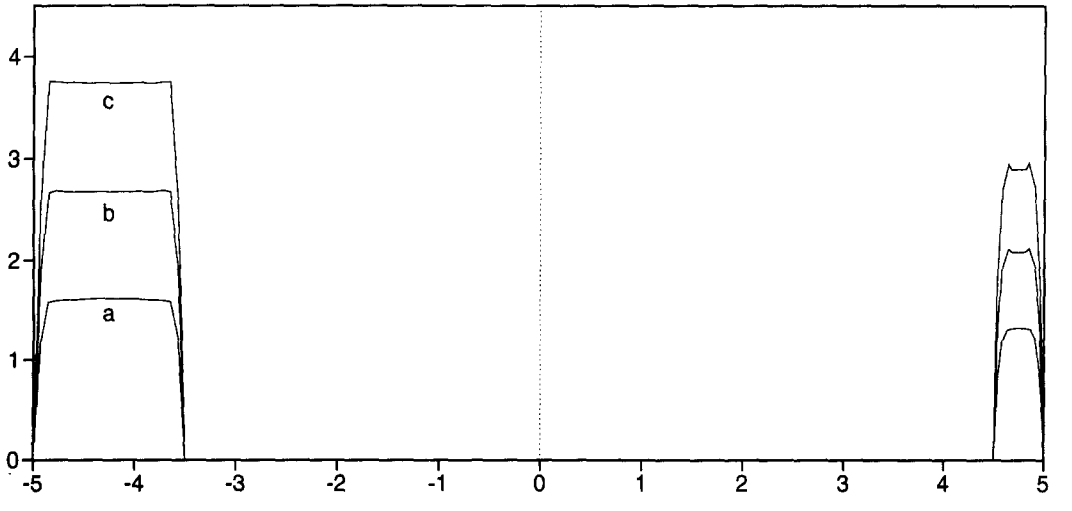

Figure 14. The development of the interface front for Re = 128, Bu = 400, Fr = 0.32 and $e = 0.20$ (MESH 3): (a) $t^* = 1.38$, (b) $t^* = 2.26$ and (c) $t^* = 3.15$. (Compare with figure 13.)

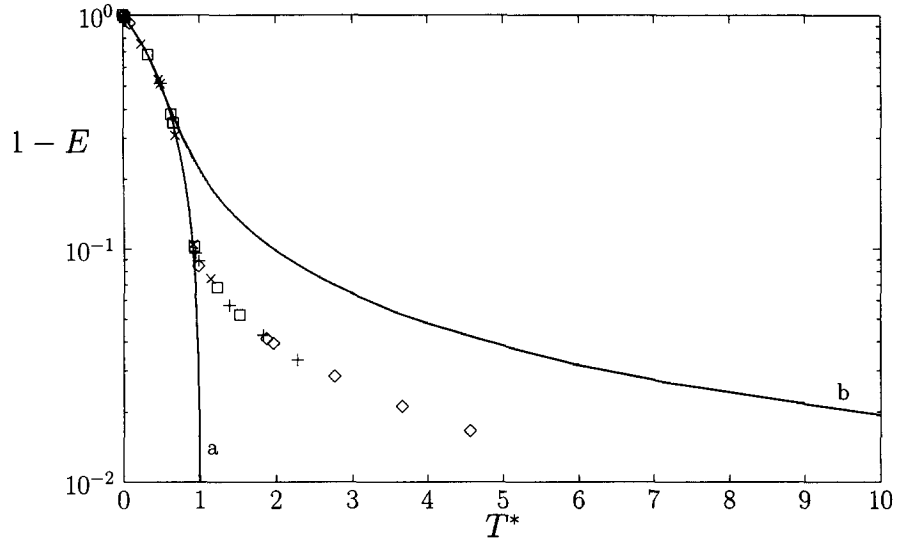

Figure 15. The displacement function, $1 - E$ vs a dimensionless time T^*: Re = 128, Bu = 400, Fr = 0.32 and $e = 0.2$. Symbols are defined as in figure 10.

forces behaves like a plug with an axial velocity that is nearly constant in the azimuthal direction. The high shear rate regions near the walls appear to lubricate the transport of this plug.

5.2.2. Displacement efficiency revisited. In the calculations at Re = 128 and Bu = 400 we can compare the displacement efficiency for various eccentricities. We have obtained results for $e = 0.0$, 0.2 and 0.5 as shown in figures 11, 15 and 16. In each figure the upper curve represents the efficiency function based on fully developed flow in the eccentric geometry as computed from a 2-D finite element method (Szabo and Hassager 1992). By comparing the figures we observe that in unidirectional flow there is a significant lowering of the function, E, as the annulus becomes more eccentric. In particular for $e = 0.5$ there is a clear reduction of E. There is, however, at Re = 128 and Bu = 400 the very different effect. Here at a non-zero eccentricity the efficiency E is largely unchanged. Thus the displacement efficiency seems to become independent of the eccentricity for large values of Bu (at Re = 128).

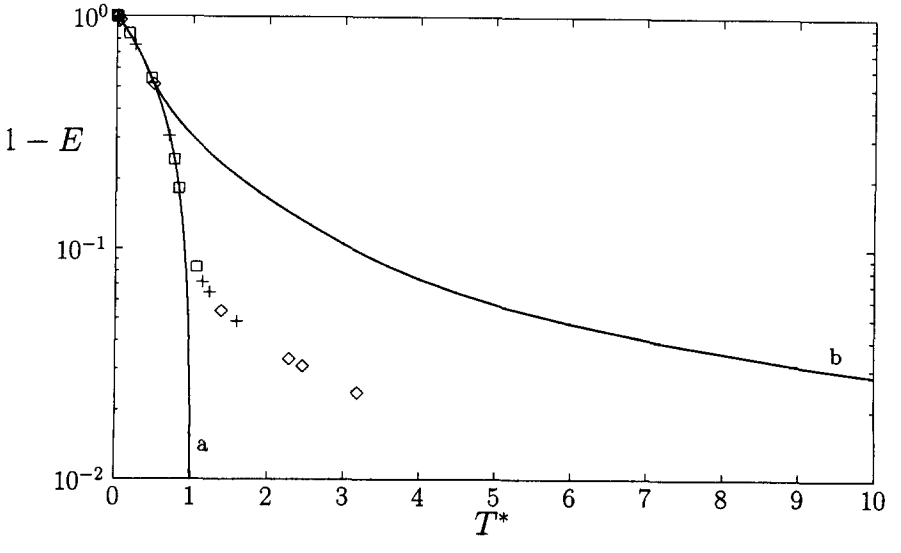

Figure 16. The displacement function, $1 - E$ vs a dimensionless time T^*: Re = 128, Bu = 400, Fr = 0.32 and $e = 0.5$. Symbols are defined as in figure 10.

6. CONCLUSIONS

The arbitrary Lagrange–Euler method may be used to simulate the displacement of one Newtonian fluid by another in a vertical annulus. The simulations support earlier experimental findings. In particular there appears to be a principle that allows the effect of the buoyancy number to be reduced or increased by adjusting the Reynolds number upwards or downwards respectively. This seems to be in agreement with a definition of the Froude number as the ratio of the Reynolds number to the Buoyancy number. Thus good displacement requires a large buoyancy number and a small Froude number.

The two-dimensional results for $Re = 128$ and $Bu = 400$ show that particles in front of the interface are transported from the wall region into the center of the annular gap whereas particles behind the interface tend to move from the center to the wall. This is in qualitative agreement with experiments made by Long (1991) and Tehrani *et al.* (1993). The detailed velocity field near the interface seems to be rather complex involving small recirculation zones.

A highly idealized lubrication theory has been proposed, that gives a simple expression for the efficiency of the displacement. The lubrication theory predicts that the displacement efficiency is independent of the ratio of the displacement length to the gap width, provided this value is sufficiently large. Comparison of the lubrication theory with the simulations suggest that the lubrication analysis tends to overpredict the displacement efficiency. The extension of this model to eccentric and deviated annuli remains as a future challenge.

Simulations of displacement in a vertical eccentric annulus show that heavier displacing fluid is transported in the azimuthal direction from the wide towards the narrow section in the annular geometry. At large Buoyancy numbers and finite Reynolds numbers, this effect seems to make the displacement efficiency independent of eccentricity.

Finally, the simulations support the prediction of the lubrication theory that the displacement efficiency becomes independent of the ratio of the displacement length to gap width for large values of this ratio. However the simulations have been performed for a limited combination of buoyancy numbers, Reynolds numbers and eccentricities. More simulations will be needed to establish the ranges of validity for this scaling behaviour.

Acknowledgements—This work was supported by the Danish Research Councils under grants 5.21.05.07 and 16-5390-1 PG. Furthermore, one of the authors (PS) was supported by a scholarship from the Technical University of Denmark (DTU). We would like to thank Dr Paul Hammond and Dr Simon Bittleston for initiating our interest in two-fluid displacement flows and Prof. B. H. A. A. van den Brule and Dr H. K. Rasmussen for many helpful discussions. Finally, we would like to thank the anonymous referees for suggestive criticism.

REFERENCES

Bird, R. B., Stewart, W. E. and Lightfoot, E. N. (1960) *Transport Phenomena*. Wiley Interscience, New York.

Brezzi, F. and Fortin, M. (1991) *Mixed and Hybrid Finite Element Methods*. Springer, New York.

Carrier, G. F. and Pearson, C. E. (1976) *Partial Differential Equations*. Academic Press, New York.

Flumerfelt, R. W. (1975) Laminar displacement of non-Newtonian fluids in parallel plate and narrow gap annular geometries. *SPE J.* **April,** 169–180.

Graves, W. G. and Collins, R. E. (1981) Non-Newtonian fluid displacement in an irregular annulus of axial symmetry. *J. Non-Newtonian Fluid Mech.* **8,** 43–58.

Huerta, A. and Liu, W. K. (1988) Viscous flow with large free surface motion. *Comp. Meth. Appl. Mech. Eng.* **69,** 277–324.

Hughes, J. R., Liu, W. K. and Zimmermann, T. K. (1981) Lagrangian–Eulerian finite element formulations for incompressible viscous flows. *Comp. Meth. Appl. Mech. Eng.* **29,** 329–349.

Jakobsen, J., Sterri, N., Saasen, A., Aas, B., Kjøsnes, I. and Vigen, A. (1991) Displacements in eccentric annuli during primary cementing in deviated wells, SPE 21686. Presented at the *Production Operations Symposium*, Oklahoma City, Oklahoma, USA, 7–9 April.

Lamb, H. (1945) *Hydrodynamics*, 6th Edition. Dover, New York.

Lockyear, C. F., Ryan, D. F. and Gunningham, M. M. (1989) Cement channelling: how to predict and prevent, SPE 19865. Presented at the *64th Annual Conference and Exhibition of the Society of Petroleum Engineers*, San Antonio, TX, USA, 8–11 October.

Long, P. J. G. (1991) Experimental studies of fluid–fluid displacement in annuli. Ph.D. thesis, University of Cambridge, Cambridge, UK.

Moore, P. L. (1974) *Drilling Practices Manual*. Penn Well Books, Tulsa.

Szabo, P. (1994) Simulation of multiphase flow. Ph.D. thesis, Institut for Kemiteknik, Danmarks Tekniske Universitet, DK 2800 Lyngby.

Szabo, P. and Hassager, O. (1992) Flow of viscoplastic fluids in eccentric annular geometries. *J. Non-Newtonian Fluid Mech.* **45,** 149–169.

Szabo, P. and Hassager, O. (1995) Simulation of free surfaces in 3-D with the arbitrary Lagrange-Euler method. *Int. J. Num. Meth. Eng.* **38,** 717–734; erratum, 1996.

Tehrani, M. A., Bittleston, S. H. and Long, P. J. G. (1993) Flow instabilities during annular displacement of one non-Newtonian fluid by another. *Experiments in Fluids* **14,** 246–256.

Tehrani, M. A., Ferguson, J. and Bittleston, S. H. (1992) Laminar displacement in annuli: a combined experimental and theoretical study, SPE 24569. Presented at the *67th Annual Conference and Exhibition of the Society of Petroleum Engineers*, Washington, DC, USA, 4–7 October.

Zienkiewicz, O. C. and Morgan, K. (1983) *Finite Elements and Approximation*. Wiley Interscience, New York.